Applied Physics Express **7**, 025204 (2014)
http://dx.doi.org/10.7567/APEX.7.025204

Atomic structure and spin polarization at the apex of tips used in spin-polarized scanning tunneling microscopy

Shigekazu Nagai[1], Koichi Hata[1], Hirofumi Oka[2], Dirk Sander[2], and Jürgen Kirschner[2]

[1]*Graduate School of Engineering, Mie University, Tsu 514-8507, Japan*
[2]*Max Planck Institute of Microstructure Physics, Weinberg 2, Halle 06120, Germany*

Received November 27, 2013; accepted January 8, 2014; published online January 29, 2014

To analyze spin-polarized scanning tunneling microscopy (STM) studies quantitatively, we evaluated the atomic structure and spin polarization at the apex of Cr/W and Fe/W tips using field ion microscopy (FIM) and field-emitted electron polarimetry, respectively. The patchwork-patterned H_2-FIM images of the Cr/W tip indicated partially developed Cr planes, and the spin polarization at the surface was 10 ± 3% at room temperature. H_2-FIM images of the Fe/W tip indicate the crystalline order of Fe layers on the W ⟨110⟩ tip, and its spin polarization was 41 ± 2%. These first results allow us to quantify the spin polarization in spin-dependent STM measurements. © 2014 The Japan Society of Applied Physics

Spin-polarized scanning tunneling microscopy and spectroscopy (SP-STM and -STS) are powerful tools for evaluating magnetic properties at the atomic level.[1–3] The contrast in SP-STM images depends on the inner product of the spin polarization vectors of a sample and the tip.[4] Their spin polarizations are sensitive to the atomic structure on their surfaces. Therefore, characterization of the spin polarization and atomic structure is useful for understanding experimentally obtained SP-STM measurements and comparing them with theoretical predictions. Although conventional W tips for STM have been characterized by field ion microscopy (FIM),[5–8] there are only few reports concerning magnetic tips, and none for Cr/W[9] and Fe/W tip,[10] which are used in SP-STM. The low evaporation field of the latter complicates the situation.

Field emission is a quantum phenomenon in which electrons at the Fermi level tunnel through a potential barrier that is deformed by an external electric field.[11] As the field-emitted electrons are extracted from the metal tip to the vacuum, their spin polarization is proportional to that of the surface at the metal tip. In our previous work, the spin polarizations at the surfaces of magnetic tips, such as Co_2MnSi/W tip[12] and an Fe_3O_4 whisker,[13] were revealed by measuring the polarization of the field-emitted electrons.

In this work, we observed the atomic structure at the apexes of magnetic tips by FIM and estimated their spin polarizations by measuring the spin polarization of field-emitted electrons for Cr/W and Fe/W tips.

Our experiments were conducted using two separate chambers with deposition systems, a standard FIM system and a field emission microscope (FEM) equipped with a sector-type spin rotator and retarding-type Mott spin polarimeter for observations of the atomic structure and measurements of the spin polarization at the surface of the tip, respectively.

Figure 1 shows a schematic diagram of a home-built FIM system for observations of the atomic structure at the tip apexes. The magnetic tip is mounted on a liquid nitrogen cold finger, which is cooled to 98 K. This is mounted on a rotatable stage, and it can be adjusted toward the MCP (micro channel plate), 50 mm away from the tip, for FIM observations. It can be rotated by 90° for alignment with the electron beam evaporator for deposition of Fe or Cr. The imaging gases, He, Ne, and H_2, can be introduced into the chamber through variable leak valves. If the ionization field of an imaging gas is higher than the evaporation field of the sample, field evaporation occurs during FIM imaging. Therefore, the ionization field of the imaging gas should be lower than the evaporation field of the sample. Because the reported values of the ionization field are 44 V/nm for He, 35 V/nm for Ne, and 20 V/nm for H_2, and those of the theoretical evaporation field are 57 V/nm for W, 34 V/nm for Fe, and 27 V/nm for Cr,[14] we use He on the order of 10^{-3} Pa for imaging the W tip. H_2 at a pressure on the order of 10^{-3} Pa is used for Cr and Fe. A LabVIEW-based program records the FIM images by a CCD camera and controls the voltage applied to the tip.

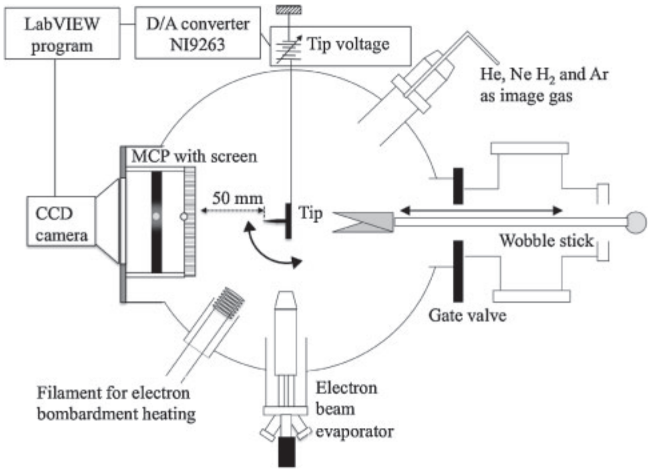

Fig. 1. Schematic diagram of field ion microscope setup at Max Planck Institute.

Figure 2 shows a schematic diagram of the electron optics for measurement of the spin polarization of the field-emitted electrons,[15] which consists of an FEM, an electrostatic and magnetostatic deflector used as a spin rotator, and a Mott spin polarimeter[16] with a gold foil 100 nm in thickness. The FEM images reflect the surface condition of the magnetic tips during the spin polarization measurements. The tip is mounted on a gimbal system and an XYZ stage to move the desired emission site onto a probe hole in a fluorescent screen. The trajectory of the electrons passing through the probe hole and two einzel lenses with two octupole deflectors is deflected by a $E \times B$ deflector used as a spin rotator. By switching between electrostatic and magnetostatic deflection, all the components of the spin polarization of field-emitted electrons can be measured by the Mott polarimeter. Electrons entering the polarimeter are accelerated to 25 keV toward a

© 2014 The Japan Society of Applied Physics

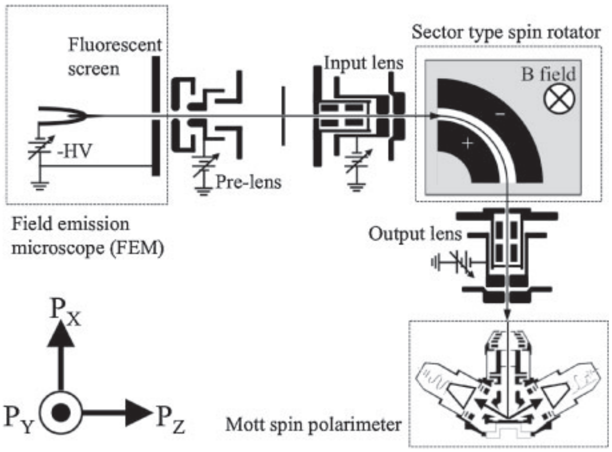

Fig. 2. Schematic diagram of electron optics for measurements of spin polarization of field-emitted electrons. The instruments consist of a FEM, an electric and magnetic deflector acting as a sector-type spin rotator, and a Mott spin polarimeter operated at 25 kV with a gold foil.

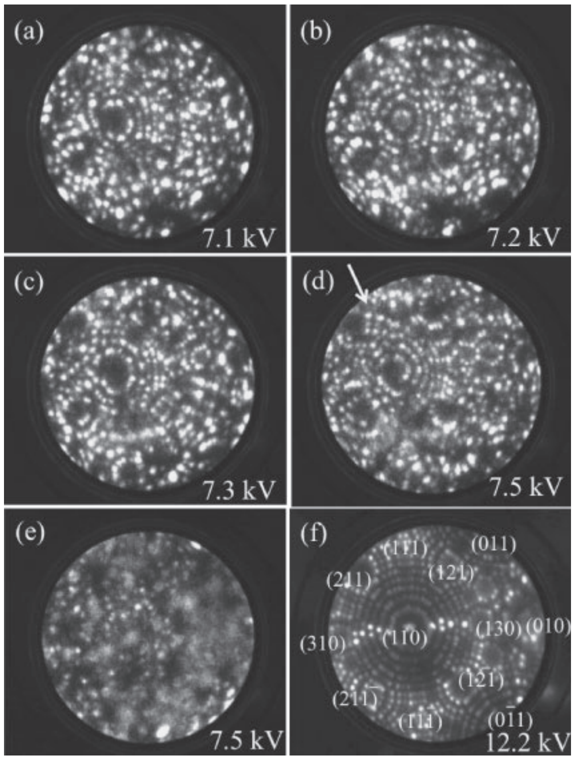

Fig. 3. Snapshot of FIM images of Fe/W tip. Sequence showing field evaporation of Fe layer appears in (a) to (e). A dramatic change in the FIM image within 1 s is apparent in the transition from (d) to (e). (f) shows a FIM image of a W tip from which the Fe layer was removed by field evaporation; the Miller index of each crystalline facet is indicated.

gold foil with a thickness of 100 nm. The scattered electrons are detected by four-channel electron multipliers (CEMs) arranged in four-fold symmetry. Inelastically scattered electrons, which have lost their kinetic energy above 600 eV, are retarded by grids placed in front of the CEMs. The asymmetry A_m in the number of electrons detected by a pair of CEMs is the summation of the spin-dependent and instrumental asymmetry. We defined the instrumental asymmetry A_i, which is attributed to the efficiencies of each detector and the incident angle of the beam axis, as the asymmetry measured with a non-polarized electron beam emitted from the substrate W tip. The spin polarization P and spin-dependent asymmetry it A_s are related by an effective Sherman function[17] S_{eff} as

$$P = \frac{A_s}{S_{eff}} = \frac{A_m - A_i}{S_{eff}}. \quad (1)$$

In this experiment, we used the S_{eff} value of 0.15 reported by Iori[18] under the same experimental conditions as we employed.

All the spatial components of the spin polarization of the field-emitted electrons from the magnetic tips were measured under a pressure of 3×10^{-8} Pa.

W tips for use as substrates were prepared by electrochemical etching of a W wire with 5 mol/l of NaOH. The surface of each W tip was cleaned by field evaporation following electron bombardment for tip heating up to 2200 K. The cleanness of the tip was confirmed by a two-fold symmetrical pattern in the He-FIM image at room temperature. Next, 70 layers of Fe or Cr were deposited by an electron beam evaporator at room temperature.

The Fe/W tip and the bare W tip were observed with imaging gases of H_2 and He, respectively, after field evaporation of Fe at 98 K, and FIM images were recorded, as shown in Figs. 3(a)–3(f). In the FIM images of the Fe/W tip, as shown in Figs. 3(a)–3(c), a concentric ring pattern is observed, which indicates a single crystalline structure at the tip apex. The FIM images show changes due to field evaporation of Fe during the observation. The Fe atoms were field-evaporated even at about 20 V/nm, which is estimated from the ionization field of H_2. In our experiment, the evaporation field was much lower than the reported theoretical value of 34 V/nm for Fe. The reason for the reduced evaporation field of Fe may be that adsorbed hydrogen atoms or molecules promote field evaporation. Such a scenario was reported by Müller.[19]

As the number of field-evaporated Fe layers reached 70, a dramatic change in the FIM image appeared, as shown in Fig. 3(e). This dramatic change suggests complete field evaporation of the deposited layers. After the field evaporation, a FIM image of the now clean W tip was observed with He as the imaging gas at a voltage of 12.2 kV, as shown in Fig. 3(f). The Miller indexes of each crystalline facet on the W tip can be identified, as shown in Fig. 3(f). Comparing Figs. 3(a)–3(d) with Fig. 3(f), one can see that the W (110) facet corresponds to the darkest part on the FIM image, which means that the deposited layer of Fe was grown epitaxially on the W tip. However, split ring patterns, indicated by an arrow in Fig. 3(d), were observed in FIM images of the Fe layers just before complete field evaporation of the Fe layer, and they indicate the properties of the first deposited layers in closest proximity to the W surfaces. Figure 4 shows an enlargement of the FIM image shown in Fig. 3(d) and a model for the atomic structure of the initially grown Fe layers. The FIM image may be interpreted as showing the coexistence of two different crystalline structures in the Fe layer on W. This could be due to an initial growth in both the bcc and bct lattices.

Figures 5(a) and 5(b) show FEM images of an Fe/W tip prepared in the instrument for spin polarization measurement and its substrate W tip after the Fe layers were removed by thermal flashing at 2000 K, respectively. The FEM image of

© 2014 The Japan Society of Applied Physics

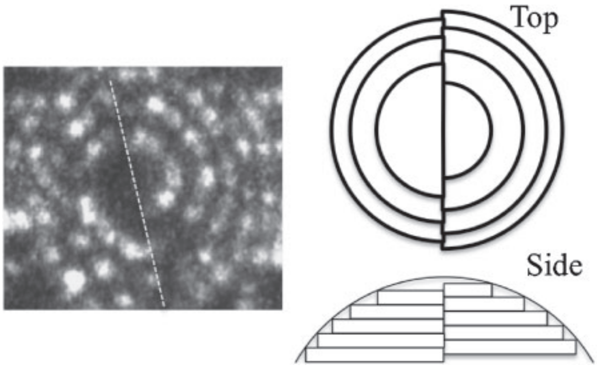

Fig. 4. Enlarged FIM image of split ring pattern in Fig. 3(d), and top and side view of models for atomic layer of Fe grown on W tip.

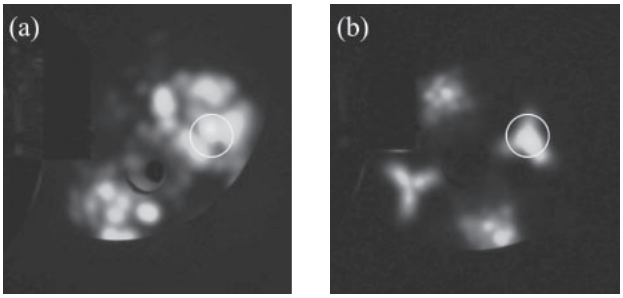

Fig. 5. FEM image of (a) Fe/W tip and (b) W tip after evaporation of Fe overlayer by thermal heating at 2000 K. Spin polarization and zero calibration of instruments were conducted using the encircled emission sites in these FEM images, respectively.

Table I. Asymmetry obtained with Fe/W tip and W tip and spin polarization for each component.

Component	X	Y	Z
A_m	0.0214	−0.0089	0.0032
A_i	−0.0151	−0.0440	−0.0158
A_s	0.365	−0.450	0.019
P (%)	24	−30	13
P_{total} (%)		41 ± 2	

the Fe/W tip in Fig. 5(a) also shows a two-fold symmetrical pattern, which corresponds to the FIM images shown in Fig. 3. Spin polarization measurement and calibration of the Mott polarimeter were conducted using the encircled emission sites in Figs. 5(a) and 5(b), respectively. Table I lists the asymmetries obtained with the Fe/W and W tip, the spin-dependent asymmetries, and the estimated spin polarization for each component. The spin polarization of field-emitted electrons from the Fe/W tip at room temperature was 41 ± 2%, where the error bar was estimated using a standard deviation of 0.0013 for each measurement of the asymmetry. This value of the spin polarization is comparable to the results obtained by Irisawa and Yamada.[20] The direction of the spin vector was 70° with respect to the tip axis. These results make the Fe/W tip interesting for studying in-plane magnetized samples.

Figure 6 shows FIM images of a Cr/W tip (left) and the substrate W tip (right) after field evaporation of the Cr layer.

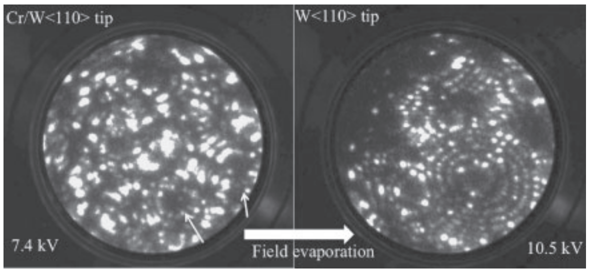

Fig. 6. FIM images of Cr/W tip before (left) and after (right) field evaporation of Cr layers.

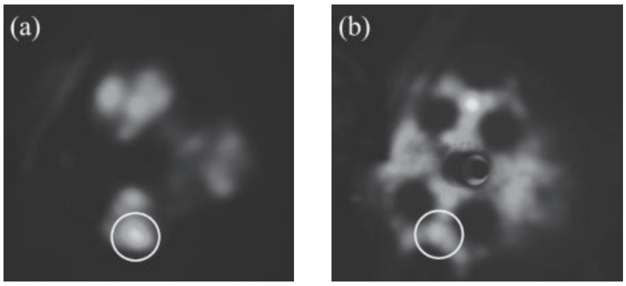

Fig. 7. FEM image of (a) Cr/W tip and (b) W tip after evaporation of Cr overlayer by thermal heating at 2000 K. Spin polarization and zero calibration of instruments were conducted using encircled emission sites in these FEM images, respectively.

In contrast to the case for the Fe/W tip, a patchwork-patterned FIM image of the Cr/W tip was observed. In Fig. 6, the parts indicated by arrows in the FIM image of the Cr/W tip show some deficient ring patterns. This suggests that the deposited Cr was grown in an island morphology, where the islands have a crystalline structure. The field evaporation rate of Cr was higher than that of Fe, which was 1 layer/s. Although some crystalline structure can be observed, the Miller index of each plane could not be identified.

FEM images of a Cr/W tip and the substrate W tip after thermal flashing at 2000 K are shown in Figs. 7(a) and 7(b), respectively. A symmetrical pattern was not identified, and some bright spots were observed in the FEM image of the Cr/W tip shown in Fig. 7(a), which reflects the island morphology of the Cr layers. As is the case for the Fe/W tip, spin polarization measurement and calibration of the instrumental asymmetry were conducted using the encircled emission site. The asymmetries obtained with the Fe/W and W tip, and the spin-dependent asymmetries and estimated spin polarization are listed in Table II. The estimated spin polarization of field-emitted electrons from the Cr/W tip at room temperature was 10 ± 3%, where the standard deviation of asymmetry was 0.003, and its direction was 80° with respect to the tip axis. This lower value of the spin polarization is ascribed to the poorer crystalline quality. For Cr(001), a spin polarization of 18% at room temperature was reported;[21] our result is lower than this experimental value. A reason might be the poor crystalline order of our Cr layer.

In this work, we investigated the atomic structures and spin polarizations at the apex of Fe/W and Cr/W tips used in SP-STM by means of FIM and field-emitted electron spin polarimetry. In the Fe/W tip, the deposited Fe layers form a single crystalline structure over the apex, except for the first

© 2014 The Japan Society of Applied Physics

Table II. Asymmetry obtained with Cr/W tip and W tip and spin polarization for each component.

Component	X	Y	Z
A_m	−0.0075	0.0211	−0.0122
A_i	−0.0190	−0.0300	−0.0150
A_s	0.0115	−0.0089	0.0028
P (%)	8	−6	2
P_{total} (%)		10 ± 3	

few layers. The spin polarization at the surface is as high as 41 ± 2%, which is attributed to the single crystalline structure of Fe. On the other hand, a FIM image of the Cr/W tip showed that the Cr layer was not well-ordered crystalline, although some hints of crystalline order were observed because of the Cr islands. Consequently, the spin polarization is as low as 10 ± 3%. These first results may allow us to prepare and characterize the structure of the magnetic tips and to quantify their spin polarization for use in spin-dependent STM.

Acknowledgment We acknowledge technical help from N. Kurowsky during this research.

1) W. Wulfhekel and J. Kirschner, Appl. Phys. Lett. **75**, 1944 (1999).
2) M. Bode, Rep. Prog. Phys. **66**, 523 (2003).
3) H. Oka, P. A. Ignatiev, S. Wedekind, G. Rodary, L. Niebergall, V. S. Stepanyuk, D. Sander, and J. Kirschner, Science **327**, 843 (2010).
4) R. Wiesendanger, Rev. Mod. Phys. **81**, 1495 (2009).
5) T. Hashizume, Y. Hasegawa, I. Kamiya, T. Ide, I. Sumita, S. Hyodo, T. Sakurai, H. Tochihara, M. Kubota, and Y. Murata, J. Vac. Sci. Technol. A **8**, 233 (1990).
6) A. Fian and M. Leisch, Ultramicroscopy **95**, 189 (2003).
7) W. Paul, Y. Miyahara, and P. Grütter, Nanotechnology **23**, 335702 (2012).
8) A.-S. Lucier, H. Mortensen, Y. Sun, and P. Grütter, Phys. Rev. B **72**, 235420 (2005).
9) G. Rodary, S. Wedekind, D. Sander, and J. Kirschner, Jpn. J. Appl. Phys. **47**, 9013 (2008).
10) S. Phark, J. A. Fischer, M. Corbetta, D. Sander, and J. Kirschner, Appl. Phys. Lett. **103**, 032407 (2013).
11) T. E. Feuchtwang, P. H. Cutler, and J. Schmit, Surf. Sci. **75**, 401 (1978).
12) S. Nagai, Y. Fujiwara, and K. Hata, Ultramicroscopy **109**, 395 (2009).
13) S. Nagai, K. Hata, M. Okada, and H. Mimura, e-J. Surf. Sci. Nanotechnol. **9**, 322 (2011).
14) T. T. Tsong, *Atom Probe Field Ion Microscopy* (Cambridge University Press, New York, 1990).
15) S. Nagai, H. Sakakibara, K. Hata, M. Okada, and H. Mimura, Ultramicroscopy **111**, 405 (2011).
16) G. C. Burnett, T. J. Monroe, and F. B. Dunning, Rev. Sci. Instrum. **65**, 1893 (1994).
17) T. J. Gay and F. B. Dunning, Rev. Sci. Instrum. **63**, 1635 (1992).
18) K. Iori, K. Miyamoto, H. Narita, K. Sakamoto, A. Kimura, S. Qiao, K. Shimada, H. Namatame, and M. Taniguchi, Rev. Sci. Instrum. **77**, 013101 (2006).
19) S. Kapur and E. W. Müller, Surf. Sci. **66**, 45 (1977).
20) T. Irisawa, T. K. Yamada, and T. Mizoguchi, New J. Phys. **11**, 113031 (2009).
21) C. Rau and S. Eichner, Phys. Rev. Lett. **47**, 939 (1981).

 © 2014 The Japan Society of Applied Physics